SWATH-MS Proteomic Analysis of Oxygen-Induced Retinopathy Reveals Novel Potential Therapeutic Targets

Maria Vähätupa,[1] Janika Nättinen,[1,2] Antti Jylhä,[1,2] Ulla Aapola,[1,2] Marko Kataja,[3] Peeter Kööbi,[1,3] Tero A. H. Järvinen,[1,4] Hannu Uusitalo,[1–3] and Hannele Uusitalo-Järvinen[1,3]

[1]Faculty of Medicine & Life Sciences, University of Tampere, Tampere, Finland
[2]The Center for Proteomics and Personalized Medicine, Tampere, Finland
[3]Eye Centre, Tampere University Hospital, Tampere, Finland
[4]Department of Musculoskeletal Disorders, Tampere University Hospital, Tampere, Finland

Correspondence: Hannele Uusitalo-Järvinen, Faculty of Medicine and Life Sciences, 33014 University of Tampere, Finland; llhauus@uta.fi.

HU and HU-J contributed equally to the work presented here and should therefore be regarded as equivalent authors.

Submitted: January 9, 2018
Accepted: May 9, 2018

Citation: Vähätupa M, Nättinen J, Jylhä A, et al. SWATH-MS proteomic analysis of oxygen-induced retinopathy reveals novel potential therapeutic targets. *Invest Ophthalmol Vis Sci*. 2018;59:3294–3306. https://doi.org/10.1167/iovs.18-23831

Purpose. Oxygen-induced retinopathy (OIR) is the most widely used model for ischemic retinopathies such as retinopathy of prematurity (ROP), proliferative diabetic retinopathy (PDR), and retinal vein occlusion (RVO). The purpose of this study was to perform the most comprehensive characterization of OIR by a recently developed technique, sequential window acquisition of all theoretical mass spectra (SWATH-MS) proteomics.

Methods. Control and OIR retina samples collected from various time points were subjected to SWATH-MS and detailed data analysis. Immunohistochemistry from mouse retinas as well as neovascular membranes from human PDR and RVO patients were used for the detection of the localization of the proteins showing altered expression in the retina and to address their relevance to human ischemic retinopathies.

Results. We report the most extensive proteomic profiling of OIR to date by quantifying almost 3000 unique proteins and their expression differences between control and OIR retinas. Crystallins were the most prominent proteins induced by hypoxia in the retina, while angiogenesis related proteins such as Filamin A and nonmuscle myosin IIA stand out at the peak of angiogenesis. Majority of the changes in protein expression return to normal at P42, but there is evidence to suggest that proteins involved in neurotransmission remain at reduced level.

Conclusions. The results reveal new potential therapeutic targets to address hypoxia-induced pathological angiogenesis taking place in number of retinal diseases. The extensive proteomic profiling combined with pathway analysis also identifies novel molecular networks that could contribute to the pathogenesis of retinal diseases.

Keywords: proteomics, mass spectrometry, oxygen induced retinopathy, angiogenesis, hypoxia

Retinal ischemic diseases, such as retinopathy of prematurity (ROP), diabetic retinopathy (DR), and retinal vein occlusion (RVO) are major causes of visual impairment and blindness in industrialized countries.[1–5] The most prominent pathological features of these diseases are abnormal angiogenesis and enhanced vascular permeability, which leads to vision loss. However, inflammation, oxidative stress, and neuronal dysfunction are also contributing to the pathogenesis of ischemic retinal diseases.

The mouse oxygen-induced retinopathy (OIR) model[6] is a well-established animal model of ROP, which shares many hallmarks with human proliferative diabetic retinopathy (PDR) as well as neovascular RVO. Thus, it is the most widely used model to study retinal ischemic diseases.[7] OIR is characterized by hyperoxia-induced vessel loss from retina followed by regrowth of vasculature and formation of preretinal neovascularization upon return to normoxia. It is considered mainly as an angiogenesis model, but neuronal damage and pathological effects on retinal glia have also been reported in OIR.[8]

Due to complex interactions between vascular, neuronal, glial, and immune cells in retinal vascular disorders, it is important to study changes in whole retinal tissue simultaneously to gain more information about the pathogenesis of retinal disease. Mass spectrometry (MS)-based proteomic profiling has become a widely-used approach to assess the development and the progression of diseases.[9] Full proteome-based approach provides an unbiased method to study changes in proteins involved in any given tissue, organ, or disease. As the OIR model is considered as the most representative model for a large number of neovascular human retinal diseases, there has been considerable interest to characterize OIR with MS-based approaches. Previous studies on rodent OIR proteome have been done with Isobaric Tags for Relative and Absolute Quantitation (iTRAQ) MS approach,[10,11] and with ion-current-based MS1 quantification approach (ICB) from rat retinas.[12] With these methods, it has been possible to quantify almost 300[10,11] and 1300 proteins from retinas,[12] respectively. In this study, a recently developed technique,[13] sequential window acquisition of all theoretical mass spectra (SWATH)-MS proteomics, was used to compare proteomes of mouse OIR model with control retina. SWATH-MS is an MS method that combines data-independent acquisition (DIA) and data-dependent acqui-

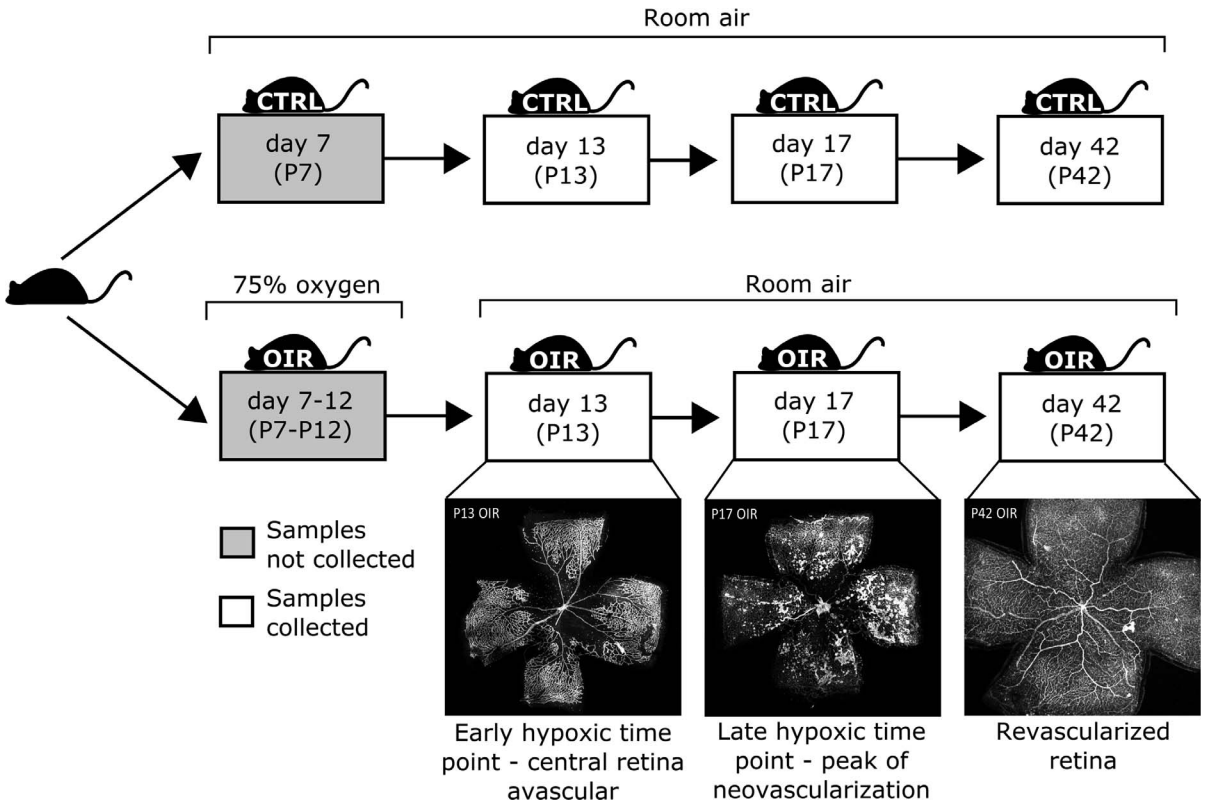

Figure 1. Outline of the study. OIR was generated by exposing the mice pups for 75% oxygen for 5 days from P7 to P12. Control and OIR retinas were collected to SWATH-MS analysis, while some retinas from each litter were used for histological examination to confirm the changes in the vasculature in OIR. Retinal vasculature was stained with Isolectin GS-IB_4. OIR samples were collected during hypoxia at P13 when central retina is avascular, at P17 when retina is partially revascularized and the neovascularization (preretinal tufts) peaks, and at P42 when retina is completely revascularized and neovascularization is regressed. Age-matching control samples were collected from mice housed in normal room air. P13 $n = 5$; P17 $n = 9$; P42 $n = 6$; P13 OIR $n = 5$; P17 OIR $n = 6$; P42 OIR $n = 7$.

sition (DDA), which iTRAQ and targeted data analysis uses, extending the throughput of proteins and data completeness.[14] Here we report the most extensive proteomic profiling of OIR to date by relatively quantifying almost 3000 unique proteins. The novel methodology used in the present study also allowed the temporal profiling of OIR proteome for the first time, while in the previous studies, it has been possible to compare the protein levels in a single time point. Immunohistochemistry was used to study the localization of differently expressed proteins in control and OIR retinas, as well as in neovascular membranes obtained from PDR and RVO patients to address the relevance of these findings to human ischemic retinopathies.

Materials and Methods

Mouse OIR Model

WT C57BL/6 mice were used for the study. Mice were housed under standard conditions with 12-hour dark/12-hour light cycle and fed with standard laboratory pellets and water ad libitum. The OIR model was generated as described in detail previously.[6,15–17] Briefly, to induce OIR, the pups at postnatal day 7 (P7) and their nursing mothers were exposed to 75% oxygen (ProOx P110 oxygen controller; Biospherix Ltd., Parish, NY, USA) for 5 days until P12 when they were returned to normal room air. Mice were sacrificed and retinas collected at P13 (early hypoxic phase), at P17 (late hypoxic phase and the peak of neovascularization), and at P42 (after vascular recovery) to assess the effect of OIR on retinal proteome. Control animals were housed under normal room air conditions and retinas were harvested at corresponding days. The study design is illustrated in Figure 1. As postnatal weight gain has been shown to affect outcome in the OIR model,[7] only the pups weighing between 6.3 and 7.5 g at P17 were included in the study. All animal experiments were conducted under ARVO Statement for the Use of Animals in Ophthalmic and Vision Research guidelines in accordance with protocols approved by the National Animal Ethics Committee of Finland.

For the proteomic analysis, eye balls were harvested into cold PBS and retinas were dissected immediately under the dissection microscope, and retinas were snap frozen with liquid nitrogen. Samples were stored in −70°C until sample preparation.

Proteomics

Chemicals and Materials. Acetonitrile (ACN), formic acid (FA), water (UHPLC-MS grade), triethylammonium bicarbonate buffer 1M (TEAB), sodium dodecyl sulfate (SDS), iodoacetamide (IAA), trifluoroacetic acid (TFA), ammonium bicarbonate (ABC), and urea were all purchased from Sigma Aldrich Corp. (St. Louis, MO, USA). Radioimmunoprecipitation assay (RIPA) cell lysis buffer, a cocktail (Halt Protease Inhibitor Cocktail), and sample clean up tips (C18) were from Thermo Fisher Scientific (San Jose, CA, USA). A kit (Bio-Rad DC) and bovine serum albumin standard were purchased from Bio-Rad (Hercules, CA, USA), and 30 kDa molecular weight cut off (MWCO) centrifugal devices were from PALL (Port Washington, NY, USA).

Sample Preparation and Analysis. Proteins were extracted by submerging tissues to 300 µL RIPA cell lysis buffer in ice and homogenized using plastic pestles and centrifuged (2400*g*/min, 5 minutes). After centrifugation, tissue samples were set in cold ultrasonic bath for 5 minutes and incubated on ice for 25 minutes. After incubation, samples were centrifuged at 21,000*g* for 20 minutes and the supernatant containing the proteins were transferred to new tube. Protein concentration was measured using Bio-Rad DC protein quantification kit. Average amount of protein recovered per sample was 253.8 ± 32.9 µg (± SD). Fifty micrograms of total protein was taken from each sample to tryptic digestion.

Samples were then subjected to reduction, alkylation, and tryptic digestion. These steps were performed as described in detail in the Supplementary Methods. For MS analysis, the samples were eluted to the same concentration and 4 µg sample was injected into NanoLC-TripleTOF (Sciex 5600+). Two replicate MS analyses were produced from each sample. Analysis of the samples was done by NanoLC-TripleTOF MS using SWATH acquisition as described in the Supplementary Methods.

Protein Identification and Quantification. As part of the SWATH analysis method, a relative protein quantification library, consisting of >3500 retinal proteins, was created using retina samples from this study. Overall library consisted of 32 different samples and 45 data-dependent analysis (DDA) runs with same LC gradient and instrument settings that were used for SWATH analyses. Library was created using Protein Pilot 4.7 (Sciex, Redwood City, CA, USA) and all DDA runs spectra were identified against Mouse UniprotKB/SwissProt protein library. Quantification was done by Peak Viewer and Marker Viewer (Sciex). False discovery rate (FDR) 1% was used in the library creation and only distinctive peptides were used in the quantification. Retention time calibration was done for all samples using 15 representative peptides from two different proteins, α-enolase (ENO1) and albumin (ALB). Five transitions per peptide and 1 to 15 peptides were used for protein quantification calculations. All statistically significant (adjusted $P < 0.05$) and other interesting proteins discussed further were subjected to manual inspection of peptides. This consisted of checking correct peak selection in the chromatogram (FDR 1%, 99% peptide confidence level), sufficient signal to noise ratio inspection (>7), and chromatogram inspection in relation to library chromatogram. Also, variation of replicate MS analysis results was calculated as means to all samples/protein. All peptides were eliminated from results processing if manual inspection requirements were not fulfilled. Proteins with missing values were excluded from consideration. Checked proteins whose quantification was based on only one specific peptide are marked with †-symbol to the graphs and tables. Most of these proteins were small proteins, meaning a small likelihood of having more than one specific peptide identified for quantification.

Western Blotting. Retinal protein lysates were run into SDS PAGE gels, transferred to polyvinylidene diflouride (PVDF) membranes, and immunoblotted with anti-Flna, anti-Myh9, and anti-glyceraldehyde-3-phosphate dehydrogenase (GAPDH) antibodies, as described in the Supplementary Methods.

Immunohistochemistry. For the retinal flat mount analysis, the eye balls were harvested at P13, P17, and P42. Eye balls were fixed with 4% paraformaldehyde (PFA) for 1 hour where after retinas were dissected, stained with isolectin (Isolectin GS-IB_4; Invitrogen, Carlsbad, CA, USA), flat mounted, and imaged via confocal microscope (LSM 700; Carl Zeiss, Oberkochen, Germany).

For immunohistochemistry, the eye balls were harvested, fixed with 4% PFA for 4 hours, and processed for paraffin embedding. Five-micrometer thick sections were subjected to antigen retrieval (Tris-EDTA, pH9), blocked and incubated either with anti-Filamin-A antibody (Cat#ab76289; Abcam, Cambridge, UK) or anti-Myh9 antibody (Cat#11128-1-AP; Proteintech, Rosemont, IL, USA) followed by horseradish peroxidase (HRP) conjugated secondary antibodies. For immunofluorescence (IF) double-staining, sections were pretreated with trypsin and incubated with anti-Myh9 antibody (Proteintech) and anti-CD31 (Cat#550274; BD BioSciences, San Jose, CA, USA) or anti-Myh9 and anti-NG2 (provided by W. Stallcup, Sanford Burnham Prebys Medical Discovery Institute, La Jolla, CA, USA),[18] followed by appropriate Alexa Fluor dye conjugated secondary antibodies (Invitrogen). Samples were imaged via confocal microscope (LSM700; Carl Zeiss).

Neovascular membranes were obtained from nine PDR and one RVO patients, who were undergoing pars plana vitrectomy. At the time of surgery, patients' mean age was 37 years (range, 27–56 years) and mean duration of diabetes was 26 years (range, 21–32 years). The protocol for collecting human tissue samples was approved by the institutional review boards of the Pirkanmaa Hospital District, and the study was conducted in accordance with the Declaration of Helsinki. All patients gave written informed consent. The fibrovascular membranes were isolated, grasped with vitreous forceps, and pulled out through a sclerotomy. Samples were immediately fixed with 10% formalin for 3 hours, transferred to 70% ethanol, and processed for paraffin embedding and immunohistochemistry. Samples were stained with anti-Myh9 antibody (Proteintech) and anti-HSA (cat #LS-B6178; LSBio, Seattle, WA, USA) followed by HRP conjugated secondary antibodies.

Statistical Analysis. Proteins were quantified and $\log_2$-transformation was applied to the data, and in addition, geometric means of replicate MS analyses were taken. No further normalization was deemed necessary. The quality of the replicate MS analyses was analyzed by analyzing the intraclass correlation (ICC), and Spearman's rank correlation was used to generate *P* values in permutation tests ($n = 1000$ permutations / replicate MS analyses).

Principal component analysis (PCA) was used to cluster the samples based on full proteomic profiles. Two-sample *t*-test was used to analyze differences between the relative protein expression levels of control and OIR retinas. Levene's test was performed for the statistically significant proteins (after *P* value adjustment), and two proteins had a *P* value < 0.05. For these proteins, the statistical significance was checked with Wilcoxon rank sum test.

Benjamini-Hochberg adjustment was used to account for multiple testing, and the significance threshold, α, was set at 0.05. All statistical analyses for the proteomics data were performed using R software version 3.2.3 (R Core Team, Foundation for Statistical Computing, Vienna, Austria) and IPA software (IPA; QIAGEN, Redwood City, CA, USA).

Results

Protein Profiles Are Associated With the Developmental Stage of the Retina

To study the protein profiles of control and OIR retinas, we first confirmed the development of OIR by staining the vasculature from retinal flat mounts at different time points (Fig. 1). With SWATH-MS quantification, we then used a library of 121,145 peptides from 32 samples, corresponding to 1,576,233 identified spectra in an assembly of 3316 protein groups using FDR of 1.0%. From this library, 2944 proteins had distinct peptides sequences with matching spectra to SWATH-MS analysis, and these proteins were quantified in all samples. Out of 2944 relatively quantified proteins, the quantification

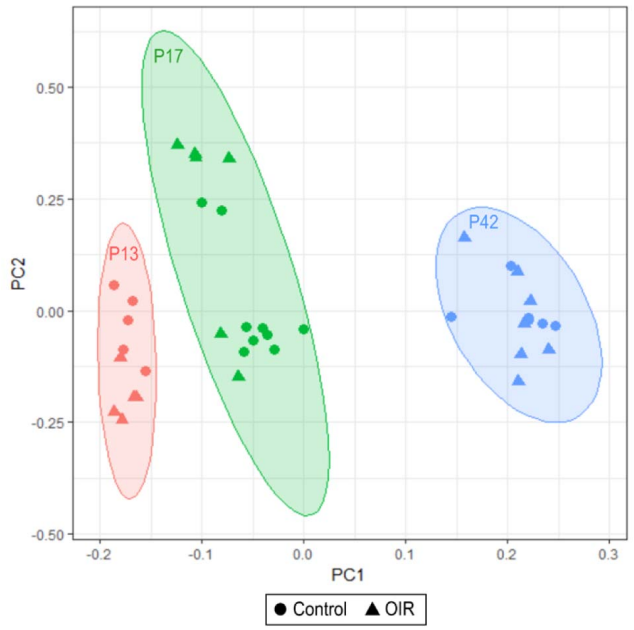

FIGURE 2. PCA shows distinct clustering of retinal proteins based on the developmental stage of the retina. The protein profiles obtained from control and OIR retinas are clearly different at P13 (*red*), P17 (*green*), and P42 (*blue*). Control (●) and OIR (▲) samples are also separated quite distinctively within the clusters at P13 and P17, but no more at P42.

was based on more than one peptide in 2177 proteins. Proteins quantified using a single peptide are marked in the figure legends. The replicate MS analysis quality checks showed that the ICC coefficient was 0.99 between the replicates. Permutation tests using Spearman's correlation showed that 94.4% of the replicate MS analyses had a $P < 0.05$, which suggests that they were of excellent quality.

For the proteomic data, we first wanted to evaluate the underlying patterns and differences between time points. PCA was performed for the whole data, and the plotting results based on the first two components suggested that there was a clear division between different time points of both control and OIR retina samples (Fig. 2). In addition, some separation was seen between control and OIR retinas at P13 and P17. At P42, the two groups were overlapping and there was no longer detectable division between control and OIR protein profiles. Taken together, the strongest cause for the differences in protein expression levels based on the first component appears to be the developmental stage of mouse retina.

Differential Expression Analysis of OIR and Control Retinas: The Induction of Crystallins by Hypoxia at P13 and Angiogenesis-Related Proteins at P17

Next, we performed differential expression analysis in order to identify proteins, which differed between control and OIR samples in specific time points. Comparison of control and OIR samples resulted in 364 differentially expressed proteins at P13, 387 at P17, and 104 at P42 ($P < 0.05$) prior to further P value adjustments. These proteins are listed in Supplementary Table S1 for P13, Supplementary Table S2 for P17, and Supplementary Table S3 for P42.

P value adjustments to account for the multiple hypotheses testing reduced the number of statistically significant results and led to 17 differentially expressed proteins at P13, 22 at P17, and none at P42. To visualize the differential expression in response to hypoxia at P13, P17, and P42, volcano plots are shown (Figs. 3A–C). In addition to visualizing the statistically significant (adjusted $P < 0.05$) proteins and their associated up- or downregulation, the plots revealed a highly upregulated group of proteins in response to hypoxia at P13 OIR (Fig. 3A). These proteins are crystallins, including members of α-, β-, and γ-crystallins. The expression levels of individual crystallins did not reach statistically significant difference after P value adjustment, but they are the most upregulated proteins in the whole data according to fold change (FC) ($\log_2$ FC 2.67–4.32) (Supplementary Fig. S1 and Supplementary Table S1). It is also noteworthy that based on FC alone, the most upregulated ($\log_2$ FC > 2) proteins at the peak of the

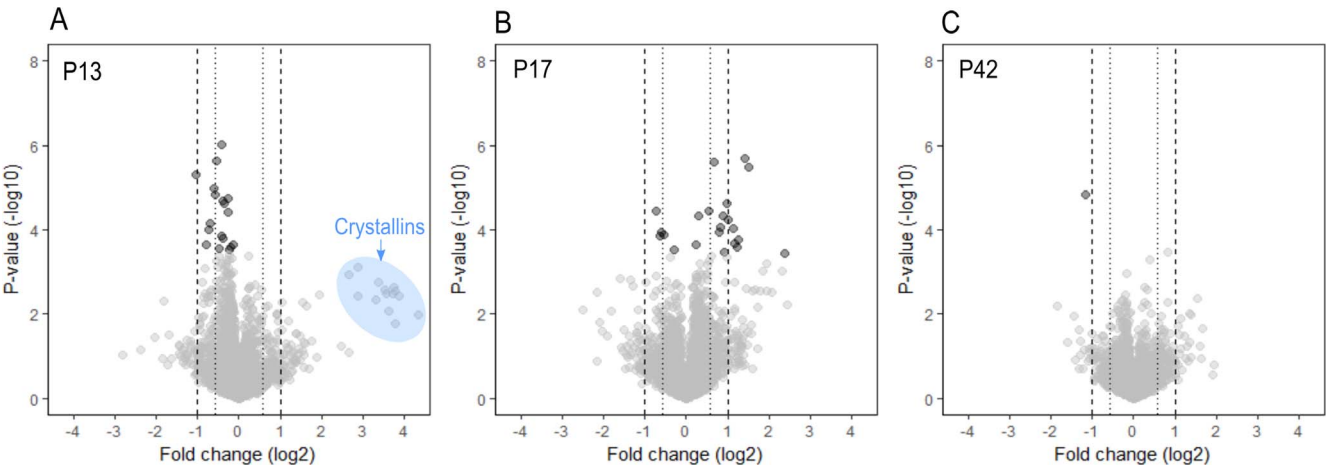

FIGURE 3. Volcano plots of the differential expression analysis. The $\log_2$ FC is displayed in the *x*-axis and the P value ($-\log_{10}$) is shown in the *y*-axis and hence, proteins in the *top right* and *left* corners are the most interesting ones as they represent the most heavily upregulated or downregulated proteins in OIR. Points with *darker gray* are proteins with an adjusted P value < 0.05. (**A**) At P13, there were 17 proteins with adjusted $P < 0.05$ and these were all downregulated in OIR samples. The blue cluster (**A**) shows the crystallins, which were noticeably upregulated although most members of the crystallin family did not reach threshold for statistical significance. (**B**) Altogether 22 proteins showed differential expression based on their adjusted $P < 0.05$ in OIR at P17. In general, more proteins were upregulated in OIR samples compared to control retinas at P17 than at other studied time points. (**C**) One protein (Cartpt) was deemed statistically significant (based on the adjusted P value) at P42, but was discarded from the results during the manual peak evaluation.

angiogenesis (at P17), were vitamin D-binding protein (Gc), α-2-HS-glycoprotein/fetuin-A (Ahsg), α-1-antitrypsin 1-4 (Serpina1d), and carboxylesterase 1C (Ces1c) (nonadjusted $P < 0.05$) (Supplementary Table S2). Of the aforementioned proteins, one (Ahsg) was also statistically significant (Fig. 3B). At P42, cocaine- and amphetamine-regulated transcript protein (Cartpt) was initially found to be statistically significant after the P value adjustment (Fig. 3C). However, this change was deemed unreliable after manual peak checking.

The heat maps of the statistically significant results at P13 and P17 show the relative expression of the proteins and the differences between control and OIR samples (Figs. 4A, 4B). Four proteins had statistically significant difference at P13 (absolute $\log_2$ FC > 0.585; i.e., FC above 1.5: abs($\log_2$(1.5)): glutamine synthetase (Glul), guanylyl cyclase GC-E (Gucy2e), cGMP-gated cation channel α-1 (Cnga1) and rod outer segment membrane protein 1 (Rom1) (Fig. 4). Substantially more proteins showed similar difference ($\log_2$ FC $>$ abs(log2(1.5)) in the expression levels between OIR and control at P17: Ahsg, annexin A2 (Anxa2), transgelin-2 (Tagln2), cell surface glycoprotein MUC18 (Mcam), tropomyosin α-4 chain (Tpm4), filamin-B (Flnb), protein SON (Son), Gpx1, vinculin (Vcl), myosin-9 (Myh9), serpin H1 (Serpinh1), filamin-A (Flna), moesin (Msn), and annexin A6 (Anxa6) (Figs. 4B, 5). Similarly, downregulated proteins at P17 OIR were Glul, prosaposin receptor GPR37 (Gpr37), sideroflexin-5 (Sfxn5), and synaptic vesicle glycoprotein 2A (Sv2a) (Fig. 4B). Significantly downregulated proteins both at P13 OIR and P17 OIR were Glul and retinaldehyde-binding protein-1 (Rlbp1). The mean expression values are illustrated in Figure 5 and in Supplementary Figure S2 for all of the statistical significant proteins (adjusted P value < 0.05). There were no proteins with altered expression level at P42 OIR after P value adjustment.

Hypoxia Induces Filamin-A Cleavage at P17 OIR

In order to validate the results from proteomic analysis of OIR, Flna and Myh9 were selected for immunoblotting. Immunoblotting with C-terminal anti-Flna antibody confirmed increased Flna expression at P17 OIR (4.6-fold compared to P17 control). In hypoxia, Flna is cleaved by calpain-proteases to generate 90 kDa C-terminal fragment that interacts with hypoxia-inducible factor-1α (HIF-1α) and promotes angiogenesis.[43] The expression of C-terminal fragment of Flna ($Flna^{CT}$) generated in the presence of hypoxia was increased 14-fold in OIR at P17 OIR (Figs. 5C, 5D). Next, the expression of Myh9 was studied in OIR by immunoblotting. A 9.6-fold increase in the expression of the Myh9 was seen at P17 OIR when compared to the expression at P17 controls (Figs. 5E, 5F).

Filamin-A and Myh9 Expression Is Increased in the Angiogenic Blood Vessels in OIR Retinas

While proteomic analysis and immunoblotting revealed an increased expression of Flna and Myh9 at P17 OIR, immunohistochemical stainings confirmed substantially stronger expression of these proteins from P17 OIR retinas than from control retinas (Fig. 5G). We observed marked increase in Flna expression in preretinal tufts and blood vessels of inner retina in the OIR retinas in comparison to controls. Also, a faint staining is seen in others cell types, presumably retinal neurons, but the expression level in neurons looks identical in control and OIR retinas. Thus, the induction of Flna expression seen in OIR at P17 is clearly from the angiogenic blood vessels.

Myh9 expression in OIR retinas was studied in detail by performing double-immunofluorescent stainings for Myh9 and endothelial cell (CD31), and pericyte (NG2) markers. Strong Myh9 expression was localized to endothelial cells and pericytes in OIR at the peak of the angiogenesis at P17. All endothelial cells expressed Myh9, while there were some pericytes negative for Myh9 at P17 OIR (Fig. 6).

Abundant Expression of Myh9 on Neovascular Membranes From Human PDR Patients

Generally, the expression levels of Myh9 reflect the overall stiffness of the tissue.[19–21] The increased matrix stiffness destabilizing endothelial cell–cell junctions impairs the endothelial barrier function and leads to enhanced endothelial permeability.[22] We next studied Myh9 and human serum albumin (HSA; i.e., marker of vascular leakage) expression on human fibrovascular membranes (using adjacent tissue sections) from vitrectomized patients with PDR and RVO. Strong fibrosis formation leads to retinal traction and ultimately to retinal detachment in RVO. The samples represent the end stage of these diseases, where substantial amount of fibrosis has been formed, but the samples still contain also regions with active pathologic angiogenesis. When only a faint expression of Myh9 is seen outside of the blood vessels, the intensity of Myh9 staining in blood vessels is also faint one (Fig. 7). Strong Myh9 expression was seen both in the blood vessels and in the matrix in some samples and then HSA starts to accumulate in the tissue. Particularly strong Myh9 expression was seen all over the fibrotic membrane in the RVO sample that contains blood vessels and massive scarring (Fig. 7). Comparison of Myh9 expression to HSA expression showed a strong positive correlation between the two; more Myh9 expressing cells (increased matrix stiffness) outside the blood vessels, more Myh9 expression (contractility and destabilization of cell–cell junctions) in the blood vessels and the more abundant vascular leakage outside the blood vessels (Fig. 7).

Ingenuity Pathway Analysis (IPA) Identifies Angiogenesis and Transforming Growth Factor-β1 (TGF-β1) Pathway As the Most Prominent Features of OIR at P17. In order to connect the differentially expressed proteins to specific pathways and biological functions, pathway analysis was performed using IPA on the proteins showing statistically significant differences in their expression between control and OIR retinas (adjusted $P < 0.05$) in each time point. The top canonical pathways connected to the 17 proteins at P13 (Fig. 4A) were phototransduction pathway ($P = 4.95e\text{-}10$) (Supplementary Fig. S3), protein kinase A signaling ($P = 2.29e\text{-}04$), and glutamine biosynthesis I ($P = 8.05e\text{-}04$). There were no unbiased activation scores < -2 or > 2 for disease and biological functions or for upstream regulators.

For the 22 proteins identified in differential expression analysis at P17 (Fig. 4B), the top canonical pathways were actin cytoskeleton signaling (activation score = 2.1, $P = 3.18e\text{-}06$), ILK signaling (activation score = −1, $P = 4.61e\text{-}05$), and glutamine biosynthesis I ($P = 1.04e\text{-}03$). We then performed the disease and biological function enrichments analyses, which showed both necrosis and cell death reduced ($P = 7.25e\text{-}04$ and $P = 6.94e\text{-}05$, both with activation score ≤ -2), while angiogenesis was increased ($P = 2.53e\text{-}04$, activation score ≥ 2). According to IPA, the increase in angiogenesis was due to the upregulation of Anxa2, Flna, Flnb, Gpx1, Mcam, Myh9, and Serpinh1. For further classification, upregulated proteins Tagln2, Vcl, Mcam, Flnb, ATP-dependent 6-phosphofructokinase (Pfkp), Myh9, and Flna are proteins involved in cell–cell adhesion (Amigo2). In addition, the upstream regulator analysis identified TGF-β1 (Tgfb1), MAP kinase-interacting serine/threonine-protein kinase 1 (Mknk1), and

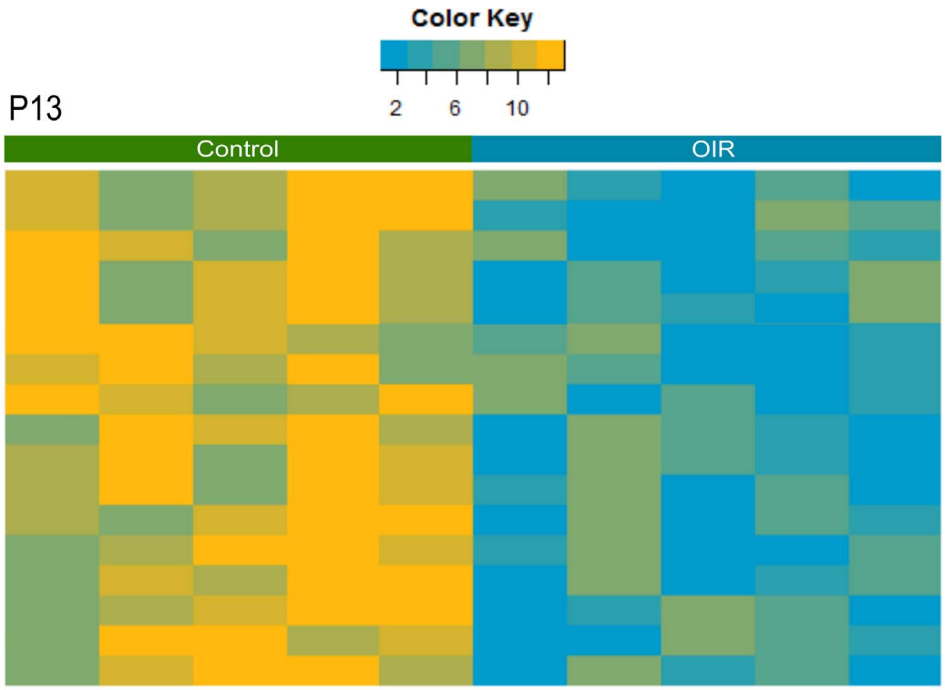

Symbol	Log2 fold change	P-value (adj.)
Cnga1	-0.7	0.02
Dnm1	-0.26	0.009
Rbbp9	-0.49	0.05
Rtcb	-0.13	0.04
Sptbn1	-0.24	0.05
Atp1b1	-0.37	0.009
Grk1	-0.58	0.009
Dusp3	-0.41	0.03
Rom1	-0.6	0.008
Nsf	-0.27	0.01
Gucy2e	-0.74	0.03
Rlbp1	-0.21	0.05
Glul	-1.05	0.005
Slc2a1	-0.4	0.04
Bsg	-0.54	0.003
Rcvrn	-0.42	0.003
Gnb1	-0.39	0.009

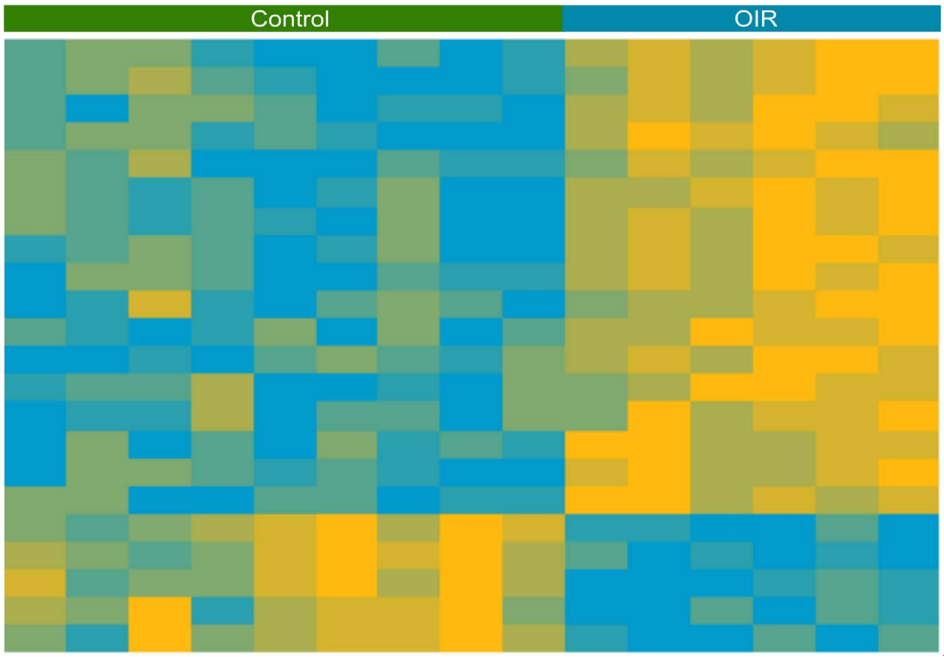

Symbol	Log2 fold change	P-value (adj.)
Pfn1	0.31	0.02
Flna	0.84	0.03
Tagln2	1.4	0.003
Flnb	1.15	0.04‡
Tpm4	1.24	0.04
Mcam	1.25	0.03
Ahsg	2.38	0.05
Vcl	0.97	0.02
Serpinh1	0.88	0.02‡
Crym	0.22	0.04
Gpx1	1.01	0.02†
Pfkp	0.54	0.02
Myh9	0.92	0.05
Msn	0.81	0.03
Son	1.12	0.03
Anxa2	1.51	0.003
Anxa6	0.68	0.003
Sv2a	-0.54	0.03
Glul	-0.74	0.02
Rlbp1	-0.3	0.04
Gpr37	-0.64	0.03
Sfxn5	-0.61	0.03

Figure 4. Heat maps of differentially expressed proteins between control and OIR retinas. Retinas from control and OIR mice were harvested at P13, P17, and P42 and processed to MS-SWATH analysis. The colors display discretized values of the relative protein expression levels as described in the color key legend. (**A**) Seventeen proteins downregulated during hypoxia at P13 OIR retinas compared to control retinas at P13 (adjusted P value < 0.05). (**B**) Twenty-two proteins up- or downregulated at P17 (neovascularization) OIR compared to control retinas at P17 (adjusted P value < 0.05). † = protein quantification based on only one specific peptide. ‡ = proteins that had significant Levene's test results (P value < 0.05), suggesting potential issues with t-test assumptions. For these proteins, the statistical significance was checked also with Wilcoxon rank sum test and results were deemed statistically significant.

MKL/myocardin-like protein 2 (Mkl2) as potential upregulated enhancers of angiogenesis (for all $P < 0.001$ and activation score ≥ 2), while brain-derived neurotrophic factor (Bdnf), Krueppel-like factor 3 (Klf3), and Myc proto-oncogene protein (Myc) were inhibited (for all $P < 0.001$ and activation score ≤ -2) (Supplementary Table S4).

Marginal Long-Term Changes in the Protein Expression Persist in OIR Retina

There were no proteins with statistically significant difference in the expression levels between OIR and control retina after P value adjustment at P42. We then performed the IPA analysis

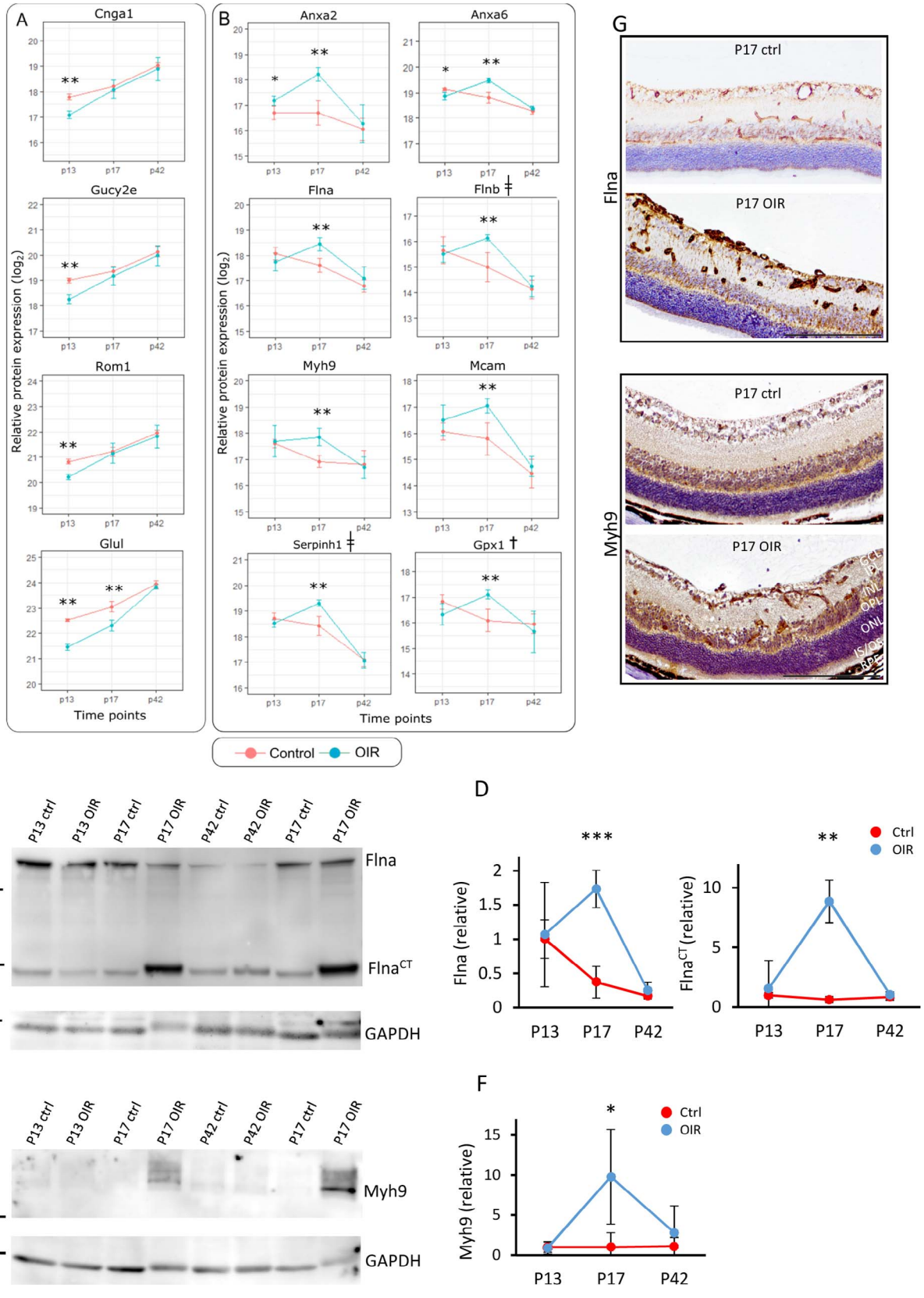

Figure 5. Differentially expressed proteins in OIR during hypoxia and angiogenesis. Mice pups were exposed to hyperoxia-induced OIR, and retinas were harvested at P13, P17, and P42. All retina samples were analyzed by MS-SWATH and the data underwent statistical analysis to compare control and OIR samples in each time point. The means and standard error bars are shown for control (*red*) and OIR (*blue*) samples for chosen proteins during hypoxia at P13 (**A**) and at the peak of neovascularization at P17 (**B**). The *asterisks* identify statistically significant differences between the two groups before *P* value adjustment (*), and after *P* value (**) adjustment. Note that Glul (**A**) is different both at P13 and at P17. (**C**) Western blot membrane immunoblotted with anti-Flna antibody shows increased Flna expression at P17 OIR and hypoxia-induced cleavage of C-

terminal fragment of Flna (Flna^{CT}). (**D**) Densitometric quantification revealed 4.6-fold induction in total Flna protein levels, while Flna^{CT} levels were increased 14-fold at P17 OIR compared to P17 control samples. (**E**, **F**) Western blotting against Myh9 and densitometric quantification showed 9.6-fold induction at P17 OIR compared to P17 control samples. (*$P < 0.05$; **$P < 0.01$; ***$P < 0.001$) (**G**) Control and OIR retinas collected at P17 were processed for immunohistochemical analysis and stained for Flna and Myh9 as described in the Materials and Methods section. Both Flna and Myh9 expression is increased in OIR retinas compared to controls. Strong expression of Flna and Myh9 can be seen from preretinal tufts (*arrows*) and from the blood vessels in inner retina in OIR. GCL, ganglion cell layer; IPL, inner plexiform layer; INL, inner nuclear layer, OPL, outer plexiform layer; ONL, outer nuclear layer; IS/OS, photoreceptor inner/outer segments; RPE, retinal pigment epithelium. *Scale bars* represent 200 μm. † = protein quantification based on only one specific peptide. ‡ = statistical significance was checked also with Wilcoxon rank sum test due to positive Levene's test results.

for proteins with nonadjusted *P* value ($P < 0.05$) as statistically significant (Supplementary Table S3). IPA analysis revealed decreased neurotransmission ($P = 6.56E\text{-}05$, activation score = −2) at P42 OIR compared to control retinas as the only significant difference between the groups. Altogether, 11 proteins in neurotransmission were involved (Supplementary Fig. S4A) and further examination revealed changes in the synaptic vesicle cycle pathway (KEGG) (Supplementary Fig. S4B). Selection of proteins upregulated at P42 OIR are illustrated in Figure 8. These are proteins associated at least with cell migration and adhesion, and retinal glial cells (Fig. 8).

Discussion

We have carried out the most comprehensive proteomics analysis of the commonly used experimental retinal angiogenesis model, OIR. The results reveal that in addition to the changes detected on proteins responding to hypoxia and those regulating angiogenesis, some changes in protein expression take place in the neuronal tissue of the retina. This is in accordance with the fact that human retinal vascular diseases are associated with neuropathy and gliopathy. Furthermore, the dysregulation of the cross talk between vasculature and retinal neuroglia and neuronal cells has been shown to contribute to the pathogenesis of DR.[23–25]

During the hypoxic phase, the most upregulated proteins were crystallins, which are small heat shock proteins that act as molecular chaperones by binding misfolded proteins to prevent their denaturation and aggregation.[26,27] They protect cells from hypoxia and maintain mitochondrial integrity.[26,28] In addition to their neuroprotective role, crystallins also have other roles in vascular biology.[29,30] αB-crystallin functions as a chaperone for VEGFA and is crucial for its proper secretion, which in turn, is crucial for endothelial cell survival in hypoxia.[28,31,32] Thus, αB-crystallin knockout mice had less VEGFA and neovascularization than WT in OIR.[31] In the eye, crystallins were originally characterized as abundant lens proteins, but they are also expressed in developing and mature retina.[28,32–34] Their expression is dramatically upregulated in numerous retinal diseases, such as mechanical injury, ischemic insults, age-related macular degeneration (AMD), uveoretinitis, and DR.[28] Concerning the potential therapeutic value of crystallins in retinal diseases, their exact functions are emerging.[27,35] Namely, the recently discovered roles for αB–crystallin in mediating TGF-β induced epithelial-mesenchymal transformation (EMT) and subretinal fibrosis in AMD,[27] while αA–crystallin providing neuroprotection for retina in DR,[35] point out the opposite therapeutic values for these crystallin-family members.[27,36]

A large number of proteins was also downregulated in response to hypoxia in retina. Among these proteins were Cnga1, Gucy2e, Rom1, and Grk1, proteins associated with phototransduction. Since rod photoreceptors are the most oxygen-dependent cells in the retina,[37] the downregulation of proteins associated with rod function is a plausible outcome in hypoxia.

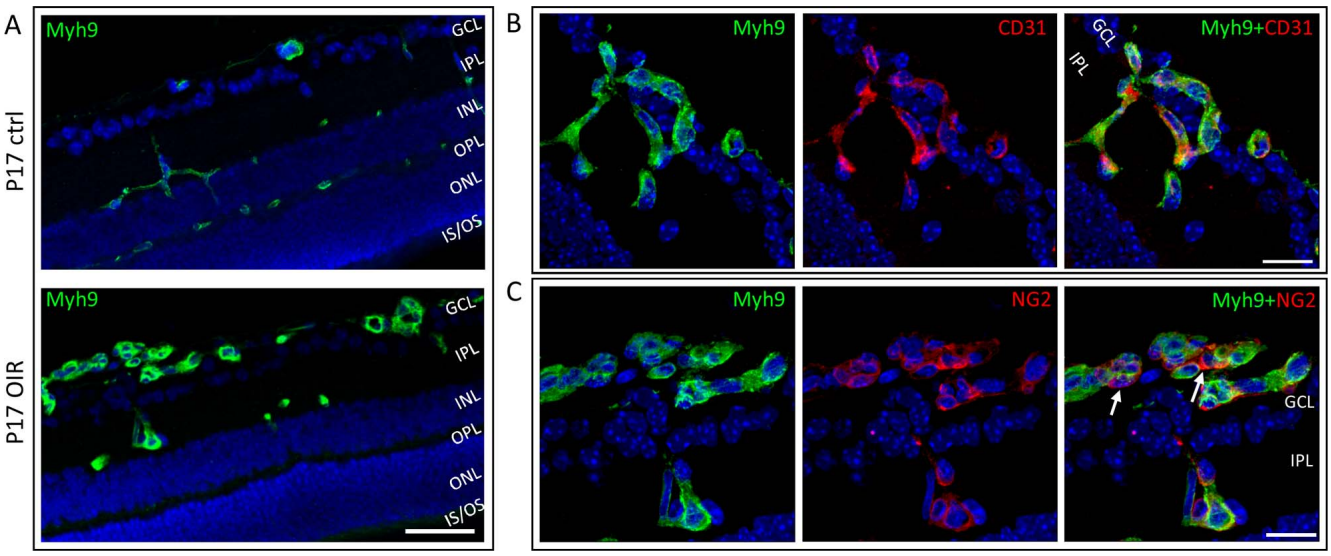

Figure 6. Myh9 is expressed in retinal blood vessels and induced by angiogenesis during OIR. (**A**) Control and OIR retinas were processed for IHC and stained for nonmuscle myosin IIA (Myh9) as described in the Materials and Methods section. Myh9 expression is confined to blood vessels in normal retina at P17. Strong Myh9 is induced in the angiogenic blood vessels at the peak of angiogenesis in OIR retina at P17. (**B**) Double-IF stainings for Myh9 and endothelial cells (CD31) (**B**) and Myh9 and pericytes (NG2) (**C**) confirmed that the Myh9 expression comes from endothelial cells and from some of the pericytes in OIR retina at P17. *Arrows* (**C**) are pointing to pericytes that do not express Myh9. GCL, ganglion cell layer; IPL, inner plexiform layer; INL, inner nuclear layer, OPL, outer plexiform layer; ONL, outer nuclear layer; IS/OS, photoreceptor inner/outer segments. *Scale bars* represent 50 μm in panel **A** and 20 μm in panels **B** and **C**.

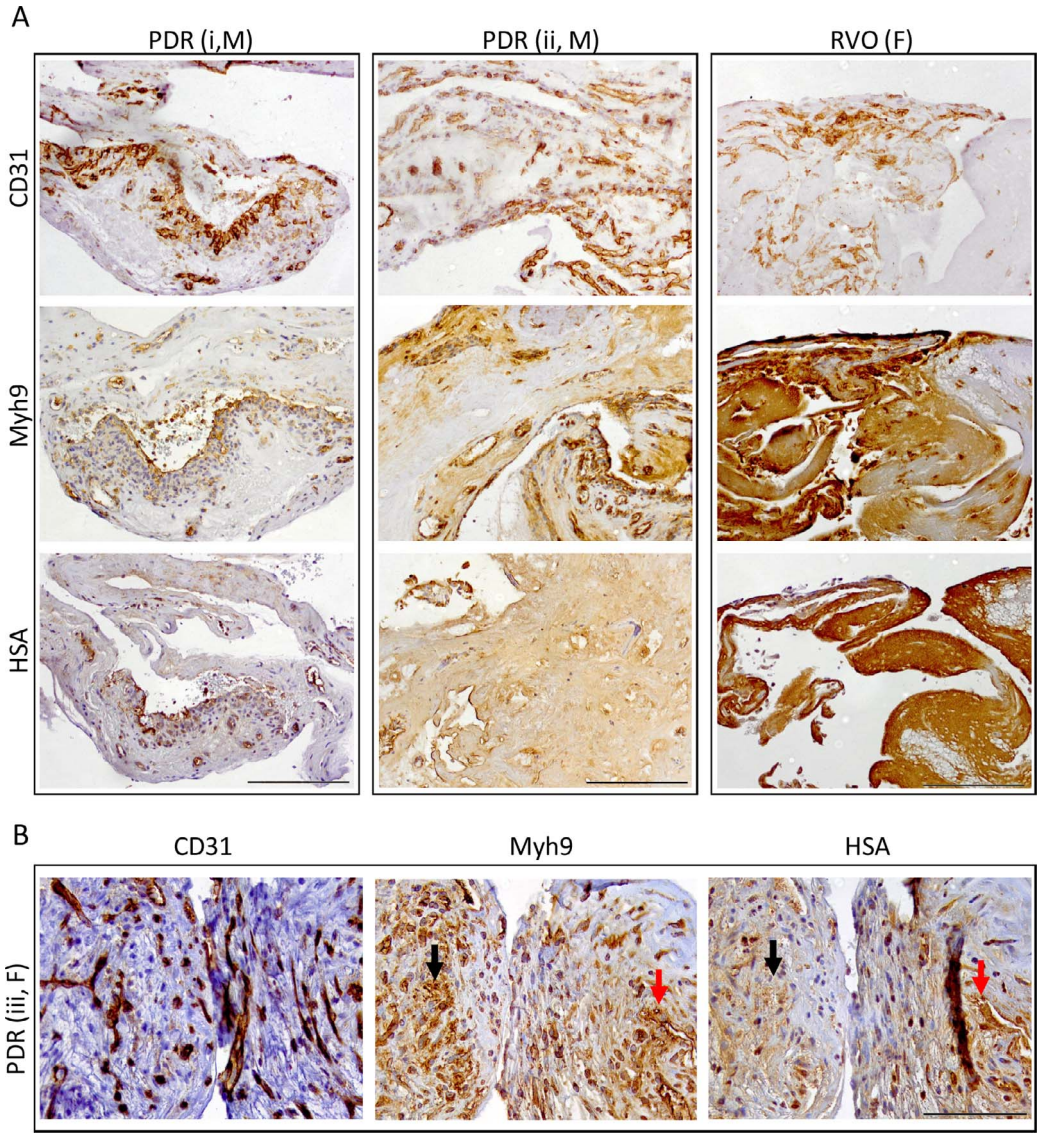

Figure 7. Myh9 is strongly expressed in human PDR and RVO fibrovascular membranes. Adjacent sections of fibrovascular membranes obtained from *pars plana* vitrectomies from PDR and RVO patients were stained for blood vessels (CD31), Myh9, and HSA. (**A**) Rather faint Myh9 expression was restricted to the blood vessels while almost no HSA accumulation was seen outside of the blood vessels in some PDR samples [PDR (i)]. Strong Myh9 expression was seen not only in the blood vessels, but also in the cells outside of the blood vessels and HSA had accumulated into the fibrovascular membrane's extracellular matrix in some PDR cases [PDR (ii)] as a sign of prominent vascular leakage. Especially strong Myh9 expression as well as substantial HSA accumulation were seen throughout the RVO sample, where strong fibrosis formation has taken place. (**B**) High magnification images from PDR patient (iii) show strong Myh9 expression in the highly vascularized area where HSA has leaked into the extracellular matrix (*arrows*). *Scale bars* represent 200 μm in panel **A** and 100 μm in panel **B**. M, male; F, female.

The most abundant changes in the retinal protein expression in OIR were seen at the peak of neovascularization at P17. Among the most upregulated proteins were plasma proteins Ahsg, Gc, Apoa1, Alb, and Tf (Supplementary Table S2). This is most probably due to increased permeability of the angiogenic blood vessels, which leads to the accumulation of plasma proteins in retinal tissue by leakage. However, some of these proteins could also have relevant biological functions, not just be bystanders by leakage, in OIR. Fetuin-A (Ahsg) as well as its cellular receptors, Anxa2 and -6, were highly upregulated in OIR. Fetuin-A is an adhesive glycoprotein that binds to Anxa2 and -6 and induces cell proliferation in its target cells.[38] Anxa2, in turn, drives angiogenesis in OIR.[38] Gc is a multifunctional glycoprotein that acts as a carrier protein for vitamin D but can also modulate certain immune and inflammatory responses.[39] Vitamin D, in turn, is known to inhibit retinal neovascularization in OIR,[40] and vitamin D receptor agonists inhibit developmental retinal angiogenesis.[41] Thus, the accumulation of Gc by the leakage from the angiogenic blood vessels could be a natural, endogenous signal to suppress angiogenesis at the time angiogenesis reaches its peak in OIR.

In line with the extensive angiogenesis taking place in retina at P17, IPA analysis revealed proteins "related to angiogenesis" being the most significantly upregulated proteins. Among these proteins were Filamins, Flna and Flnb. In hypoxia, oxygen-sensing prolyl hydroxylase domain protein 2 (PHD2) inactivation rapidly upregulates Flna expression.[42] Flna, in turn, interacts physically with HIF-1α and promotes angiogenesis.[43] Hypoxia induces calpain-dependent cleavage of Flna, and its C-terminal fragment ($Flna^{CT}$) accumulates in the nucleus and facilitates the nuclear localization of HIF-1α.[43] Our study shows that hypoxia induces Flna cleavage, that is, $Flna^{CT}$

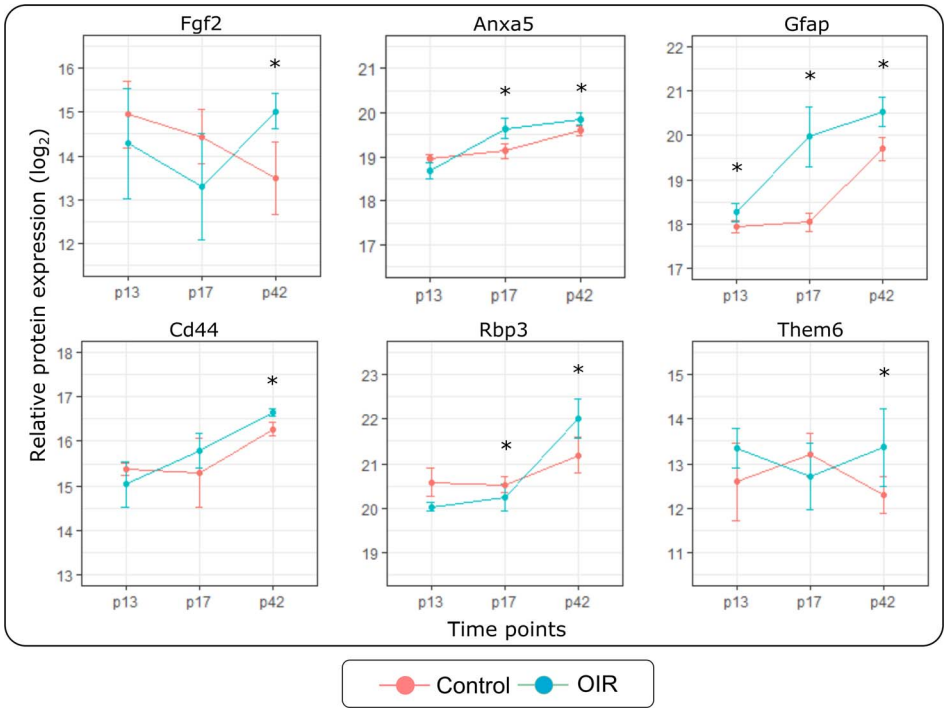

Figure 8. Selection of upregulated proteins at P42 OIR. Mice were exposed to OIR, and control and OIR retinas were harvested at P13, P17, and P42. Samples were analyzed by MS-SWATH, and the data underwent statistical analysis to compare control and OIR samples. The means and standard error bars are shown for control (*red*) and OIR (*blue*) samples for chosen proteins involved in cell migration and adhesion (Fgf2, Anxa5, CD44) and retinal glial cells (Gfap). Rbp3 has a critical role in visual cycle. The *asterisks* identify statistically significant differences between the two groups before *P* value adjustment (*P* value < 0.05).

generation in OIR. Very recently it was shown that blocking the calpain-dependent cleavage of Flna impairs tumor cell proliferation and migration.[44] Furthermore, it is worth noting that Flna also interacts with small GTPase, R-Ras,[45,46] the master regulator of vascular permeability in angiogenesis[46–50] and the gene needed for proper endothelial lumenogenesis.[51] The interaction between Flna and R-Ras is crucial for controlling vascular permeability in angiogenesis.[45,46] R-Ras, in turn, regulates vascular permeability in OIR and the reduced expression of R-Ras is associated with vascular leakage in PDR.[16] The interaction between R-Ras and Flna takes place with the N-terminal part of Flna.[45] Thus, selective blocking of the C-terminal cleavage of Flna ($Flna^{CT}$) could potentially be therapeutic in ischemic retinal diseases with pathological angiogenesis.

Another angiogenesis-related protein that stands out is Myh9. Myh9 gene encodes for Myosin 9, a heavy chain of Myosin IIA, a cytoskeletal contractile protein.[52] In general, the expression levels of Myh9 reflect the stiffness of the tissue; cells in stiff tissues express plenty of Myh9, while the cells in nonstiff tissues express low levels of Myh9.[19–21] In addition to the stiffness of the tissue, cell migration induces high mechanical strains on the cells as their "pierce" through extracellular matrix. Thus, the migrating cells upregulate the expression of Myh9 to make themselves more rigid to withstand the mechanical forces placed on them during the migratory process,[19–21] but their enhanced contractility destabilizes endothelial cell–cell junctions and impairs endothelial barrier function, resulting in increased vascular permeability.[22,53,54] Angiogenesis is essentially a cell migratory process and as shown in this study, the upregulation of the Myh9 takes place in the angiogenic endothelial cells in the retina. Thus, the induction of Myh9 during the peak of angiogenesis in OIR is plausible phenomenon, but could also be highly relevant as the increased vascular leakage is a hallmark in OIR. We also studied samples obtained from human PDR and RVO patients and showed that the vascular leakage in these diseases correlates with the amount of Myh9 expression in this area. Endothelial cell contractility (i.e., enhanced Myh9 expression) increases not only with cell migration, but also with the increased matrix stiffness resulting in increased endothelial permeability due to impaired endothelial barrier function.[22,53–55] Thus, the changes in matrix stiffness and the resultant endothelial cell contractility could be highly relevant for large number of neovascular retinal diseases associated with pathological leakage from the blood vessels.

Myh9 also regulates angiogenesis via controlling the production of VEGFA in ischemia-driven arteriogenesis[56] as well as controlling nucleolin translocalization.[57] Nucleolin is primarily a nuclear protein that translocates to cell surface in angiogenesis.[57–59] The different antagonists of nucleolin, among them Myh9 antibodies, have been shown to inhibit tumor angiogenesis by stabilizing the pathological vasculature,[57,59] which enhances tissue oxygenation.[59] The modest increase (log_2 FC 0.23) in nucleolin expression seen by MS in OIR at P17 suggests that the effects of nucleolin in angiogenesis is merely related to its translocation from nucleus to cell surface than increase in its expression level.

The present proteomics approach quantifies complete expression pattern of almost 3000 proteins and thus provides strong value to identify pathways involved in OIR. Using the upstream regulator analysis with IPA, the most potential and activated upstream regulator driving angiogenesis was TGF-β1. This is in accordance with previous studies showing TGF-β1 upregulation in OIR.[60] Interestingly, conditional ocular deletions of TGF-β signaling results in pronounced structural changes of retinal capillaries and a phenotype similar to human DR.[61,62] The upstream regulator analysis identified Mkl2 and

Mknk1 as enhancers of angiogenesis in OIR. Mkl2, a transcriptional coactivator, regulates conserved TGF-β signaling pathway.[63] Mice deficient for Mkl2 die at the early embryonic state, and Mkl2$^{-/-}$ ECs have defects in cytoskeletal organization and cell adhesion.[63] Mkl2/TGF-β pathway is required for the maturation and stabilization of embryonic vasculature,[63–65] but also for the myofibroblast transformation and EMT induction.[66,67] The enhanced TGF-β signaling taking place in vasculature leads to the endothelial-mesenchymal transition (EndMT), a process that has many similarities with EMT.[68,69] The transformed endothelial cells have high vascular permeability, further driving inflammation and by thus perpetuating the incomplete repair state.[69] This inflammation–TGF-β circuit in vasculature also promotes fibrosis in the surrounding tissue, and it is largely irreversible.[68,69] The recently identified association between TGF-β signaling and αβ-crystallin in the EMT and subretinal scarring,[27] the massive induction of crystallins by hypoxia and the subsequent activation of TGF-β/Mkl2-signaling pathways in OIR provide clues about the potential interplay that leads to retinal fibrosis in the human neovascular diseases of retina.

Another upstream regulator potentially enhancing angiogenesis in OIR is Mknk1/MNK1. Mknk1 is a kinase that exclusively phosphorylates a cap-binding subunit of the eIF4F translation initiation complex, eIF4E, and selectively facilitating translation of proliferation, migration, and survival promoting mRNAs, among them VEGFA.[70] Inhibition of eIF4E phosphorylation, in turn, suppressed angiogenesis.[71] In retina, eIF4E interacts with 4E-bp1, which expression is enhanced in retina by diabetes-induced hyperglycemia and necessary for VEGFA expression.[72,73] Our results suggest that blocking MNK-eIF4E pathway could be a potential target for blocking pathological angiogenesis in retinal diseases.

We included the late OIR-time point, P42, in our study to assess whether hypoxic exposure and subsequent neovascularization cause permanent changes in the protein expression in the retina. Very little is known about the long-term effects of OIR on retina, although the information could be useful to understand the prognosis of ROP. The disruption of the retinal morphology as well as decrease in neuronal function have been reported after OIR.[74] Our IPA analysis revealed decreased neurotransmission at P42 OIR retinas. Further examination revealed changes in the synaptic vesicle cycle pathway (KEGG) (Supplementary Fig. S4).

The present proteomics analysis revealed novel pathways that might contribute to the development of pathological angiogenesis in OIR. Furthermore, we were able to identify molecular interplay between the proteins induced by hypoxia and then by subsequent angiogenesis in OIR. They could be potential druggable targets of retinal diseases inflected with hypoxia and neovascularization.

Acknowledgments

The authors thank Saara Lähdekorpi and Marianne Karlsberg for excellent technical assistance; William B. Stallcup (Sanford Burnham Prebys Medical Discovery Institute, La Jolla, CA, USA) for providing the NG2 antibody. The imaging of the IF samples was done with a confocal microscope provided by Tampere Imaging Facility, BioMediTech, and Faculty of Medicine and Life Sciences, University of Tampere.

Supported by Academy of Finland, Finnish Diabetic Research Foundation, Diabetes Wellness Foundation, Tampere Tuberculosis Foundation, Pirkanmaa Hospital District Research Foundation, Finnish Eye Foundation, Finnish Cultural Foundation, Mary and Georg C. Ehrnrooth's Foundation, Päivikki and Sakari Sohlberg Foundation, Elsemay Björn Fund, and TEKES.

Disclosure: **M. Vähätupa**, None; **J. Nättinen**, None; **A. Jylhä**, None; **U. Aapola**, None; **M. Kataja**, None; **P. Kööbi**, None; **T.A.H. Järvinen**, None; **H. Uusitalo**, None; **H. Uusitalo-Järvinen**, None

References

1. Reynolds JD. Insights in ROP. *Am Orthopt J*. 2014;64:43–53.
2. Fong DS, Aiello LP, Ferris FL III, Klein R. Diabetic retinopathy. *Diabetes Care*. 2004;27:2540–2553.
3. Laouri M, Chen E, Looman M, Gallagher M. The burden of disease of retinal vein occlusion: review of the literature. *Eye (Lond)*. 2011;25:981–988.
4. Laatikainen L, Ojamo M, Rudanko SL, et al. Improving visual prognosis of the diabetic patients during the past 30 years based on the data of the Finnish Register of Visual Impairment. *Acta Ophthalmol*. 2016;94:226–231.
5. Gissler M, Ojamo M, Ritvanen A, Uusitalo H. Pediatric ocular disorders and visual handicap in Finland—what do the registers tell? *Duodecim*. 2017;133:159–166.
6. Smith LE, Wesolowski E, McLellan A, et al. Oxygen-induced retinopathy in the mouse. *Invest Ophthalmol Vis Sci*. 1994; 35:101–111.
7. Stahl A, Connor KM, Sapieha P, et al. The mouse retina as an angiogenesis model. *Invest Ophthalmol Vis Sci*. 2010;51: 2813–2826.
8. Vessey KA, Wilkinson-Berka JL, Fletcher EL. Characterization of retinal function and glial cell response in a mouse model of oxygen-induced retinopathy. *J Comp Neurol*. 2011;519:506–527.
9. Cifani P, Kentsis A. Toward comprehensive and quantitative proteomics for diagnosis and therapy of human disease. *Proteomics*. 2017;17:1600079.
10. Kim SJ, Jin J, Kim YJ, Kim Y, Yu HG. Retinal proteome analysis in a mouse model of oxygen-induced retinopathy. *J Proteome Res*. 2012;11:5186–5203.
11. Zhou L, Xinling L, Koh SK, Xiaorong L, Beuerman RW. Quantitative proteomic analysis of retina in oxygen-induced retinopathy mice using iTRAQ with 2D NanoLC-nanoESI-MS/MS. *Jiomics*. 2011;1:226–235.
12. Tu C, Beharry KD, Shen X, et al. Proteomic profiling of the retinas in a neonatal rat model of oxygen-induced retinopathy with a reproducible ion-current-based MS1 approach. *J Proteome Res*. 2015;14:2109–2120.
13. Gillet LC, Navarro P, Tate S, et al. Targeted data extraction of the MS/MS spectra generated by data-independent acquisition: a new concept for consistent and accurate proteome analysis. *Mol Cell Proteomics*. 2012;11:O111.016717.
14. Rosenberger G, Koh CC, Guo T, et al. A repository of assays to quantify 10,000 human proteins by SWATH-MS. *Sci Data*. 2014;1:140031.
15. Uusitalo-Järvinen H, Kurokawa T, Mueller BM, Andrade-Gordon P, Friedlander M, Ruf W. Role of protease activated receptor 1 and 2 signaling in hypoxia-induced angiogenesis. *Arterioscler Thromb Vasc Biol*. 2007;27:1456–1462.
16. Vähätupa M, Prince S, Vataja S, et al. Lack of R-Ras leads to increased vascular permeability in ischemic retinopathy. *Invest Ophthalmol Vis Sci*. 2016;57:4898–4909.
17. Vähätupa M, Cordova ZM, Aittomäki S, et al. Furin deficiency in myeloid cells leads to attenuated revascularization in a mouse-model of oxygen-induced retinopathy. *Exp Eye Res*. 2018;166:160–167.
18. Huang FJ, You WK, Bonaldo P, Seyfried TN, Pasquale EB, Stallcup WB. Pericyte deficiencies lead to aberrant tumor vascularization in the brain of the NG2 null mouse. *Dev Biol*. 2010;344:1035–1046.

19. Cho S, Irianto J, Discher DE. Mechanosensing by the nucleus: from pathways to scaling relationships. *J Cell Biol*. 2017;216:305–315.
20. Discher DE, Smith L, Cho S, Colasurdo M, Garcia AJ, Safran S. Matrix mechanosensing: from scaling concepts in 'omics data to mechanisms in the nucleus, regeneration, and cancer. *Annu Rev Biophys*. 2017;46:295–315.
21. Irianto J, Pfeifer CR, Xia Y, Discher DE. SnapShot: mechanosensing matrix. *Cell*. 2016;165:1820–1820.e1.
22. Bordeleau F, Mason BN, Lollis EM, et al. Matrix stiffening promotes a tumor vasculature phenotype. *Proc Natl Acad Sci U S A*. 2017;114:492–497.
23. Barber AJ. A new view of diabetic retinopathy: a neurodegenerative disease of the eye. *Prog Neuropsychopharmacol Biol Psychiatry*. 2003;27:283–290.
24. Kern TS. Interrelationships between the retinal neuroglia and vasculature in diabetes. *Diabetes Metab J*. 2014;38:163–170.
25. Nakahara T, Mori A, Kurauchi Y, Sakamoto K, Ishii K. Neurovascular interactions in the retina: physiological and pathological roles. *J Pharmacol Sci*. 2013;123:79–84.
26. Diokmetzidou A, Soumaka E, Kloukina I, et al. Desmin and αB-crystallin interplay in the maintenance of mitochondrial homeostasis and cardiomyocyte survival. *J Cell Sci*. 2016;129:3705–3720.
27. Ishikawa K, Sreekumar PG, Spee C, et al. αB-Crystallin regulates subretinal fibrosis by modulation of epithelial-mesenchymal transition. *Am J Pathol*. 2016;186:859–873.
28. Kannan R, Sreekumar PG, Hinton DR. Alpha crystallins in the retinal pigment epithelium and implications for the pathogenesis and treatment of age-related macular degeneration. *Biochim Biophys Acta*. 2016;1860:258–268.
29. Sinha D, Klise A, Sergeev Y, et al. βA3/A1-crystallin in astroglial cells regulates retinal vascular remodeling during development. *Mol Cell Neurosci*. 2008;37:85–95.
30. Zhang C, Gehlbach P, Gongora C, et al. A potential role for β- and γ-crystallins in the vascular remodeling of the eye. *Dev Dyn*. 2005;234:36–47.
31. Kase S, He S, Sonoda S, et al. αB-crystallin regulation of angiogenesis by modulation of VEGF. *Blood*. 2010;115:3398–3406.
32. Kannan R, Sreekumar PG, Hinton DR. Novel roles for α-crystallins in retinal function and disease. *Prog Retin Eye Res*. 2012;31:576–604.
33. Vazquez-Chona F, Song BK, Geisert EE Jr. Temporal changes in gene expression after injury in the rat retina. *Invest Ophthalmol Vis Sci*. 2004;45:2737–2746.
34. Smolich BD, Tarkington SK, Saha MS, Grainger RM. Xenopus γ-crystallin gene expression: evidence that the γ-crystallin gene family is transcribed in lens and nonlens tissues. *Mol Cell Biol*. 1994;14:1355–1363.
35. Ruebsam A, Dulle JE, Myers AM, et al. A specific phosphorylation regulates the protective role of αA-crystallin in diabetes. *JCI Insigbt*. 2018;3:e97919.
36. Nagaraj RH, Nahomi RB, Mueller NH, Raghavan CT, Ammar DA, Petrash JM. Therapeutic potential of α-crystallin. *Biochim Biophys Acta*. 2016;1860:252–257.
37. Cringle SJ, Yu DY, Alder VA. Intraretinal oxygen tension in the rat eye. *Graefes Arch Clin Exp Ophthalmol*. 1991;229:574–577.
38. Huang B, Deora AB, He KL, et al. Hypoxia-inducible factor-1 drives annexin A2 system-mediated perivascular fibrin clearance in oxygen-induced retinopathy in mice. *Blood*. 2011;118:2918–2929.
39. Delanghe JR, Speeckaert R, Speeckaert MM. Behind the scenes of vitamin D binding protein: more than vitamin D binding. *Best Pract Res Clin Endocrinol Metab*. 2015;29:773–786.
40. Albert DM, Scheef EA, Wang S, et al. Calcitriol is a potent inhibitor of retinal neovascularization. *Invest Ophthalmol Vis Sci*. 2007;48:2327–2334.
41. Merrigan SL, Kennedy BN. Vitamin D receptor agonists regulate ocular developmental angiogenesis and modulate expression of dre-miR-21 and VEGF. *Br J Pharmacol*. 2017;174:2636–2651.
42. Segura I, Lange C, Knevels E, et al. The oxygen sensor PHD2 controls dendritic spines and synapses via modification of filamin A. *Cell Rep*. 2016;14:2653–2667.
43. Zheng X, Zhou AX, Rouhi P, et al. Hypoxia-induced and calpain-dependent cleavage of filamin A regulates the hypoxic response. *Proc Natl Acad Sci U S A*. 2014;111:2560–2565.
44. Salimi R, Bandaru S, Devarakonda S, et al. Blocking the cleavage of filamin A by calpain inhibitor decreases tumor cell growth. *Anticancer Res*. 2018;38:2079–2085.
45. Griffiths GS, Grundl M, Allen JS III, Matter ML. R-Ras interacts with filamin A to maintain endothelial barrier function. *J Cell Physiol*. 2011;226:2287–2296.
46. Sawada J, Urakami T, Li F, et al. Small GTPase R-Ras regulates integrity and functionality of tumor blood vessels. *Cancer Cell*. 2012;22:235–249.
47. Sawada J, Komatsu M. Normalization of tumor vasculature by R-Ras. *Cell Cycle*. 2012;11:4285–4286.
48. Ichimiya H, Maeda K, Enomoto A, Weng L, Takahashi M, Murohara T. Girdin/GIV regulates transendothelial permeability by controlling VE-cadherin trafficking through the small GTPase, R-Ras. *Biochem Biophys Res Commun*. 2015;461:260–267.
49. Komatsu M, Ruoslahti E. R-Ras is a global regulator of vascular regeneration that suppresses intimal hyperplasia and tumor angiogenesis. *Nat Med*. 2005;11:1346–1350.
50. Zhao K, Li X, Lin B, et al. Oroxyloside inhibits angiogenesis through suppressing internalization of VEGFR2/Flk-1 in endothelial cells. *J Cell Physiol*. 2018;233:3454–3464.
51. Li F, Sawada J, Komatsu M. R-Ras-Akt axis induces endothelial lumenogenesis and regulates the patency of regenerating vasculature. *Nat Commun*. 2017;8:1720.
52. Pecci A, Ma X, Savoia A, Adelstein RS. MYH9: structure, functions and role of non-muscle myosin IIA in human disease. *Gene*. 2018;664:152–167.
53. Huynh J, Nishimura N, Rana K, et al. Age-related intimal stiffening enhances endothelial permeability and leukocyte transmigration. *Sci Transl Med*. 2011;3:112–122.
54. Lampi MC, Reinhart-King CA. Targeting extracellular matrix stiffness to attenuate disease: from molecular mechanisms to clinical trials. *Sci Transl Med*. 2018;10:eaao0475.
55. Kohn JC, Lampi MC, Reinhart-King CA. Age-related vascular stiffening: causes and consequences. *Front Genet*. 2015;6:112.
56. Morrison AR, Yarovinsky TO, Young BD, et al. Chemokine-coupled β2 integrin-induced macrophage Rac2-Myosin IIA interaction regulates VEGF-A mRNA stability and arteriogenesis. *J Exp Med*. 2014;211:1957–1968.
57. Huang Y, Shi H, Zhou H, Song X, Yuan S, Luo Y. The angiogenic function of nucleolin is mediated by vascular endothelial growth factor and nonmuscle myosin. *Blood*. 2006;107:3564–3571.
58. Christian S, Pilch J, Akerman ME, Porkka K, Laakkonen P, Ruoslahti E. Nucleolin expressed at the cell surface is a marker of endothelial cells in angiogenic blood vessels. *J Cell Biol*. 2003;163:871–878.
59. Fogal V, Sugahara KN, Ruoslahti E, Christian S. Cell surface nucleolin antagonist causes endothelial cell apoptosis and normalization of tumor vasculature. *Angiogenesis*. 2009;12:91–100.

Investigative Ophthalmology & Visual Science

60. Yingchuan F, Chuntao L, Hui C, Jianbin H. Increased expression of TGF-β1 and Smad 4 on oxygen-induced retinopathy in neonatal mice. *Adv Exp Med Biol*. 2010;664: 71–77.
61. Braunger BM, Leimbeck SV, Schlecht A, Volz C, Jagle H, Tamm ER. Deletion of ocular transforming growth factor β signaling mimics essential characteristics of diabetic retinopathy. *Am J Pathol*. 2015;185:1749–1768.
62. Schlecht A, Leimbeck SV, Jagle H, Feuchtinger A, Tamm ER, Braunger BM. Deletion of endothelial transforming growth factor-β signaling leads to choroidal neovascularization. *Am J Pathol*. 2017;187:2570–2589.
63. Li J, Bowens N, Cheng L, et al. Myocardin-like protein 2 regulates TGFβ signaling in embryonic stem cells and the developing vasculature. *Development*. 2012;139:3531–3542.
64. Trembley MA, Velasquez LS, de Mesy Bentley KL, Small EM. Myocardin-related transcription factors control the motility of epicardium-derived cells and the maturation of coronary vessels. *Development*. 2015;142:21–30.
65. Menendez MT, Ong EC, Shepherd BT, et al. BRG1 (Brahma-Related Gene 1) promotes endothelial Mrtf transcription to establish embryonic capillary integrity. *Arterioscler Thromb Vasc Biol*. 2017;37:1674–1682.
66. Crider BJ, Risinger GM Jr, Haaksma CJ, Howard EW, Tomasek JJ. Myocardin-related transcription factors A and B are key regulators of TGF-β1-induced fibroblast to myofibroblast differentiation. *J Invest Dermatol*. 2011;131:2378–2385.
67. Gasparics A, Sebe A. MRTFs- master regulators of EMT. *Dev Dyn*. 2017;247:396–404.
68. Dejana E, Hirschi KK, Simons M. The molecular basis of endothelial cell plasticity. *Nat Commun*. 2017;8:14361.
69. Schwartz MA, Vestweber D, Simons M. A unifying concept in vascular health and disease. *Science*. 2018;360:270–271.
70. Zhan Y, Guo J, Yang W, et al. MNK1/2 inhibition limits oncogenicity and metastasis of KIT-mutant melanoma. *J Clin Invest*. 2017;127:4179–4192.
71. Liu Y, Sun L, Su X, Guo S. Inhibition of eukaryotic initiation factor 4E phosphorylation by cercosporamide selectively suppresses angiogenesis, growth and survival of human hepatocellular carcinoma. *Biomed Pharmacother*. 2016;84: 237–243.
72. Dennis MD, Kimball SR, Fort PE, Jefferson LS. Regulated in development and DNA damage 1 is necessary for hyperglycemia-induced vascular endothelial growth factor expression in the retina of diabetic rodents. *J Biol Chem*. 2015;290: 3865–3874.
73. Miller WP, Mihailescu ML, Yang C, et al. The translational repressor 4E-BP1 contributes to diabetes-induced visual dysfunction. *Invest Ophthalmol Vis Sci*. 2016;57:1327–1337.
74. Tokunaga CC, Mitton KP, Dailey W, et al. Effects of anti-VEGF treatment on the recovery of the developing retina following oxygen-induced retinopathy. *Invest Ophthalmol Vis Sci*. 2014;55:1884–1892.

Investigative Ophthalmology & Visual Science